Surface cyclotron resonance on InSb in Voigt configuration

U. Merkt
Institut für Angewandte Physik, Universität Hamburg, Jungiusstrasse 11, D-2000 Hamburg 36, Federal Republic of Germany
(Received 29 April 1985)

Magnetic fields parallel to space-charge layers on semiconductors define a crossed-field configuration with strong electric fields. Analytical expressions for the resulting hybrid electric-magnetic surface band structure and its optical transitions are derived in the triangular-well approximation of the electrostatic potential. The results of the one-band effective-mass approximation are extended to a two-level model that accounts for the nonparabolicity of narrow-band-gap semiconductors such as InSb. In the hybrid surface band structure, electrons with bulklike wave functions exist, allowing the experimental study of conduction-band cyclotron resonance in crossed fields. This is done in a wide range of frequencies, magnetic fields, and inversion electron densities, i.e., electric field strengths. The experimental results are discussed within the proposed models and are compared with experiments on other semiconductors. Specifically, the destruction of the Landau quantization in crossed electric and magnetic fields is investigated, both theoretically and experimentally; polarons are also studied. This is possible because of the absence of coupled plasma cyclotron—LO-phonon modes in the present degenerate electron system.

I. INTRODUCTION

In the bulk of metals and semiconductors the energy spectrum of electrons in a magnetic field is split into highly degenerate Landau levels. Near surfaces the degeneracy is lifted and magnetic surface levels are formed. In metals and semimetals the Fermi energy by far exceeds the cyclotron energy and magnetic surface levels are occupied.[1–5] In semiconductors the situation is different and surface levels must be populated by different means. This can be achieved by an electric field that forces the electrons toward the surface. However, a surface electric field quantizes the motion of electrons into electric subbands[6] and coupling of the magnetic and electric quantization must be considered.[7–10] The resulting hybrid electric-magnetic subbands are of electric type[11,12] if the electric subband energies exceed the cyclotron energy, and vice versa.[13–15]

We have recently demonstrated that in hybrid subbands not only surface bound electrons, but also bulklike electrons, exist.[10] The latter can be regarded as bulk electrons in crossed electric and magnetic fields. This paper is mainly concerned with these electrons.

In previous work on optical absorption in crossed electric and magnetic fields interband absorption was studied. The breakdown of selection rules was predicted[16] and was observed in Ge.[17,18] No corresponding experiments exist for intraband absorption, though much theoretical effort has been devoted to this subject.[19,20] In a two-level model[19] the breakdown of the Landau quantization in strong electric fields and the experimentally observed transition from oscillatory interband magnetoabsorption to exponential Franz-Keldysh absorption[21] could be explained.

In the volume of semiconductors in the crossed-field configuration there is a transition from a discrete Landau spectrum to a continuous eigenvalue spectrum when the electric field is increased. However, near surfaces the electrons can become quantized into electric subbands and a transition from discrete Landau to discrete electric subband states is obtained. Therefore, in the present system we can experimentally study, how cyclotron resonances are affected by a transverse electric field and how the transition to electric subband states takes place.

The bulklike states in the hybrid surface band structure are interesting also for different reasons. The effective density of electrons in inversion layers is high ($\sim 10^{16}$—10^{19} cm^{-3}), but cyclotron resonance is not plasma shifted as in the corresponding Voigt configuration in bulk samples.[22] Also, no collective cyclotron—LO-phonon modes are observed,[23] but single electron excitations are.[24,25] This allows the experimental study of polarons in a system with variable and high electron densities. We make use of this advantage and study screening effects of the electron—LO-phonon interaction that have theoretically been predicted for electrons in inversion layers.[26] Because the bulk electrons are described by volume wave functions, we are also able to decide on wave-function arguments that were put forward in the literature.[26] This is done by comparison with experimental data obtained in Faraday configuration.[27]

In Sec. II we present simple models for the surface band structure and its electric dipole transitions in the crossed-field configuration. In Sec. II A we consider the classical trajectories that give an intuitive picture for the motion of surface electrons. In Sec. II B we treat the one-band effective-mass approximation that we extend in Sec. II C to the two-level model that accounts for the nonparabolicity of narrow-gap semiconductors. In Sec. III we give a brief description of our samples and the experimental setup. In Sec. IV we discuss the experimental results and compare them with our models. We conclude with a summary in Sec. V.

II. THEORY

A. Classical trajectories

In Fig. 1 classical trajectories of surface electrons in crossed electric and magnetic fields are depicted. In Fig. 1(a) the electric limit ($B=0$) is shown. As initial conditions we choose the coordinate $(0,0,z_i)$ and two velocities $(0,\pm v_y,0)$. In the absence of the surface at $z=0$ the electron accelerates in the electric field and the motion is unbound (dashed line). Quantum-mechanically this corresponds to a continuous spectrum. In the presence of a surface, that is assumed to be ideally smooth, the electron is periodically reflected from the surface and follows a so-called skipping trajectory[1,8] (solid line). For the two initial velocities $\pm v_y$ the same trajectory is followed in opposite directions.

In Fig. 1(b) the magnetic limit ($F_S=0$) is depicted. We choose similar initial conditions as in the electric limit. Unlike in the electric limit, the velocities $\pm v_y$ lead to completely different trajectories. Depending on the sign of the velocity, the Lorentz force either pulls the electron into the bulk of the semiconductor ($v_y>0$) or it binds it to the surface ($v_y<0$) as did the Coulomb force eF_s in the electric limit for all electrons. Thus, in a magnetic field two different trajectories are obtained, namely cyclotron circles identical with those of bulk electrons and skipping trajectories that are similar to the trajectories in a surface electric field. Most characteristic for magnetic trajectories are their center coordinates $z_0=v_y/\omega_c$. For bulk electrons they lie far inside the semiconductor, but may even lie outside the semiconductor for magnetically bound electrons ($z_0<0$).

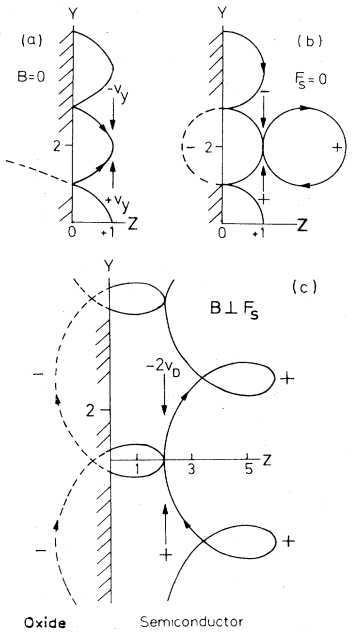

FIG. 1. Classical trajectories of electrons near ideally reflecting surfaces at $z=0$. (a) Electric field $F_s||z$, (b) magnetic field $B||x$, and (c) crossed fields $F_s\perp B$. Dashed lines indicate trajectories in the absence of the surface. Arrows and signs ± indicate initial conditions and resulting trajectories. In (c) the coordinates are normalized with v_D/ω_C.

Figure 1(c) shows trajectories in crossed fields.[28] The most characteristic feature now is the constant drift velocity $v_D=F_s/B$ by which all electrons drift transverse to both fields. The trajectories for the initial velocities $v_y=\pm 2v_D$ are depicted in the figure. As in the magnetic limit in Fig. 1(b), the classical trajectory lies entirely in the interior of the semiconductor if the initial velocity is positive. Such electrons will again behave like bulk electrons. For negative velocities the cycloide may hit the surface and the corresponding electrons can not complete their free motion (dashed line). Again the electron is periodically reflected and its motion is represented by a relatively complicated skipping trajectory that is not included in Fig. 1(c). Such electrons are bound to the surface by the combined action of the electric and the magnetic field and the corresponding quantized levels are referred to as hybrid surface states.[7]

We want to emphasize two important characteristics of surface electrons in crossed fields that are revealed by their classical trajectories. Firstly, there are two kinds of electrons. Depending on the sign of the initial velocity we have bulk electrons and bound electrons. Secondly, all electrons periodically come back to their initial z coordinate. To achieve this kind of motion, the bulklike electrons do not hit the surface, whereas the bound electrons do. The behavior of the bulklike electrons is rather unphysical, if strong electric fields or vanishing magnetic fields are considered. In such fields an electric type of motion with continuous acceleration along the electric field [see Fig. 1(a), dashed line] and reflection at the surface is expected for all electrons.

For a free electron in vacuum the transition to such an electric type of motion is obtained from the relativistic equation of motion.[29] The drift velocity has a physical meaning only if it is less than the light velocity. Up to the light velocity the motion remains magnetic, i.e., periodic with the cyclotron frequency ω_c. The motion becomes electric, if the drift velocity reaches the light velocity.

For semiconductor electrons the analogous transition is obtained only in a two-level approach for the valence and conduction bands.[19,30] Then a limiting velocity $(\varepsilon_g/2m_0^*)^{1/2}$ analogous to the light velocity in free space is obtained with the band gap ε_g and the effective mass at band edge m_0^* However, unlike in free space an unbound trajectory like that in Fig. 1(a) (dashed line) cannot be obtained near a surface. Instead of this, a transition to an electric subband state [Fig. 1(a), solid line] occurs.

B. One-band model

1. Crossed-field results

In our model the electrostatic surface potential is approximated by a triangular potential well.[31] This simple model ignores screening and many body effects and only provides a rough approximation to a self-consistent potential. For space-charge layers on InSb self-consistent theories only exist in the absence of magnetic fields.[32,33]

The merit of the triangular approximation is that the hybrid surface band structure and the optical transitions can be calculated almost analytically and that many interesting aspects of the coupled electric and magnetic quantization can be explained in simple terms.

In our coordinate system the $z=0$ plane separates the oxide from the semiconductor ($\mathbf{F}_s \| \mathbf{z}$, $\mathbf{B} \| \mathbf{x}$). Ignoring spin, the Schrödinger equation becomes

$$\left[\frac{(\mathbf{p}+e\mathbf{A})^2}{2m^*}+eF_s z\right]\Psi=E\Psi \tag{1}$$

with the boundary condition $\Psi(z=0)=0$ for an infinite potential barrier. In the gauge $\mathbf{A}=(0,-Bz,0)$ the total electric and magnetic surface potential only depends on the z coordinate and we look for solutions in the form

$$\Psi(x,y,z)=D(z)\exp(ik_x x+ik_y y)\ . \tag{2}$$

This ansatz reduces Schrödinger's equation to a one-dimensional differential equation. It is convenient to define dimensionless variables. Referring to the electric and the magnetic fields, the problem has two characteristic lengths and two characteristic energies. The lengths are the subband width L and the cyclotron radius l:

$$L=\left[\frac{\hbar^2}{2m^*eF_s}\right]^{1/3},\quad l=\left[\frac{\hbar}{eB}\right]^{1/2}. \tag{3}$$

The characteristic energies are the electric zero-point energy E_0 and the cyclotron energy $\hbar\omega_c$:

$$E_0\simeq\frac{\hbar^2}{m^*L^2}\ ,\quad \hbar\omega_c=\frac{\hbar^2}{m^*l^2}\ . \tag{4}$$

Dimensionless variables are introduced by the cyclotron radius l, the cyclotron energy $\hbar\omega_c$, and the wave vector $k_D=m^*F_s/\hbar B$ of the drift velocity $v_D=F_s/B$. The dimensionless space coordinate is defined by

$$\zeta=\sqrt{2}(z-z_0)/l\ ,\quad z_0=l^2(k_y-k_D)\ , \tag{5}$$

where z_0 will turn out as center coordinate of the motion. A dimensionless energy parameter is defined by

$$\nu+\tfrac{1}{2}=(E-E_{2D})/\hbar\omega_c+(z_0/l)^2/2 \tag{6}$$

with the $2D$ dispersion $E_{2D}=\hbar^2(k_x^2+k_y^2)/2m^*$. The equation for $D(\zeta)$ then has the standard form of the differential equation of the parabolic cylinder (Weber) functions,[34]

$$\frac{d^2D_\nu}{d\zeta^2}-(\tfrac{1}{4}\zeta^2-\nu-\tfrac{1}{2})D_\nu(\zeta)=0\ . \tag{7}$$

The motion of surface electrons is thus described by "oscillations" $D_\nu(\zeta)$ around the center coordinate z_0.

Before we discuss the wave functions and the hybrid energy levels it is illustrative to make clear the physical meaning of the two dimensionless parameters k_Dl and z_0/l that enter Eq. (7) through Eqs. (5) and (6).

The parameter k_Dl is the ratio of the electrostatic energy eF_sl and the cyclotron energy $\hbar\omega_c$ and is also related to the characteristic lengths:

$$k_Dl=\frac{eF_sl}{\hbar\omega_c}=\frac{1}{2}\left[\frac{l}{L}\right]^3. \tag{8}$$

Note, that $k_Dl=\frac{1}{2}$ describes maximum coupling of the electric and magnetic quantization ($L=l$). The coordinate $z_0/l=k_yl-k_Dl$ of Eq. (5) is given by the momentum $\hbar k_y$ and a constant shift due to the crossed-field configuration and describes the center of the wave functions or corresponding classical trajectories.

Only parabolic cylinder functions D_ν that vanish at infinity ($z\to+\infty$) provide solutions to our problem. The allowed indices ν_i follow from the boundary condition $D_\nu(z=0)=D_\nu(-\sqrt{2}z_0/l)=0$. Therefore, the zeros of the parabolic cylinder functions must be known to obtain the wave functions and the energy eigenvalues (see Appendix A).

The energy eigenvalues for the center coordinate z_0/l are obtained from the allowed indices ν_i from Eq. (6). As is necessary for a complete solution, an infinite number $i=0,1,\ldots$ of states exists for each center coordinate (see Appendix A). The energy spectrum in the hybrid subband i is

$$E_{i,k_x,z_0}=\frac{\hbar^2(k_x^2+k_D^2)}{2m^*}+(\nu_i+\tfrac{1}{2})\hbar\omega_c+eF_sz_0\ . \tag{9}$$

The quantum numbers are the wave vector k_x, the hybrid subband index i, and the center coordinate z_0/l. Note that the index ν_i is a function of the center coordinate z_0/l. Unlike bulk Landau states, the levels are not highly degenerate, but the energy depends on the distance z_0/l from the surface.

In Fig. 2(a) wave functions of the ground hybrid subband are depicted for various center coordinates z_0/l. For center coordinates $z_0/l\gg+1$, wave functions are practically Gaussian and identical with bulk Landau functions. Because the center of oscillation lies far inside the semiconductor, the electron does not feel the influence of the surface. Negative center coordinates mean that the electron is strongly bound to the surface. Then the wave function is very similar to the one of a purely magnetically or electrically bound electron. This becomes clear from a comparison with the corresponding Airy solution.[2,31]

The ground hybrid subband is shown in Fig. 2(b) for various parameters k_Dl. The energy eigenvalues are given versus the center coordinate z_0/l. The magnetic surface levels ($k_Dl=0$) are directly given by the indices $\nu_i(z_0/l)$ of the parabolic cylinder functions (see Appendix A). In crossed electric fields, a straight line must be added to the magnetic levels according to Eq. (9). This shifts the subband minimum to finite and even to negative center coordinates with increasing k_Dl parameters, i.e., increasing electric or decreasing magnetic field strengths.

We now calculate the transition matrix elements for electric dipole radiation in the crossed-field configuration. Two polarization vectors of the incident light $\mathbf{E}$ are considered. The polarization can either be parallel to the surface (parallel excitation) or it can be perpendicular to it (perpendicular excitation). In both cases, the polarization is perpendicular to the magnetic field (see insert in Fig. 3). Optical transitions with polarization parallel to the mag-

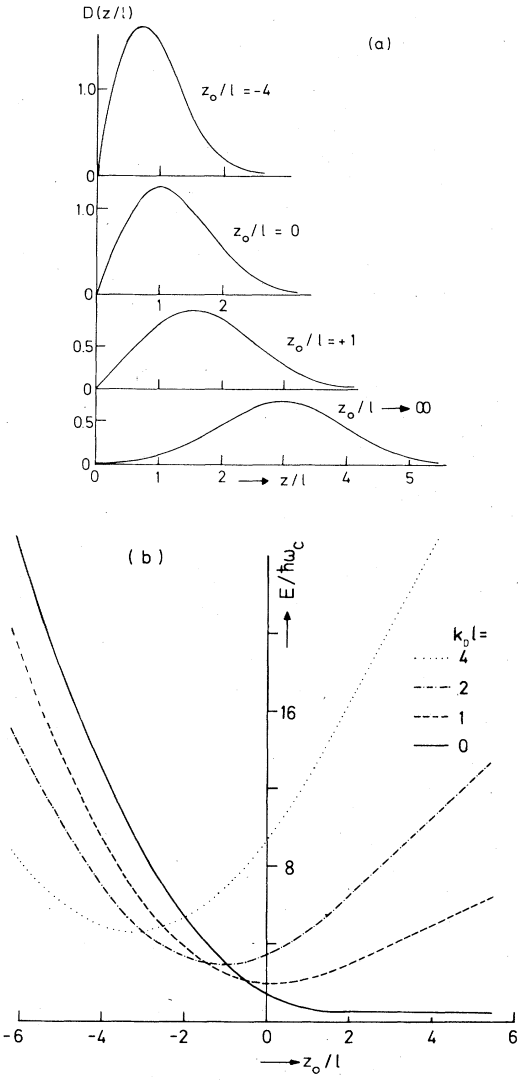

FIG. 2. (a) Normalized wave functions in the ground hybrid subband for various center coordinates z_0/l. (b) Ground hybrid subbands ($i=0$, $k_x=0$) for various parameters $k_D l$. For $k_D l=0$ magnetic surface levels are obtained, and for $k_D l \to \infty$ electric subband parabolas are obtained.

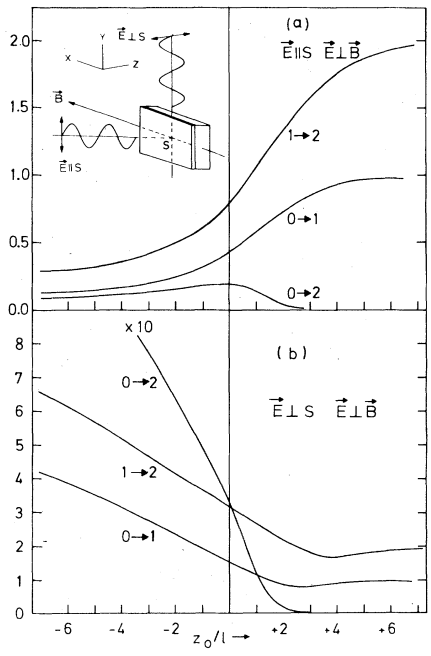

FIG. 3. Optical transition strengths for (a) parallel and (b) perpendicular excitation. Paralled ($\mathbf{E}\|S$) and perpendicular ($\mathbf{E}\perp S$) excitation is defined in the inset. Transition strengths are normalized to cyclotron resonance of bulk electrons ($0\to1$).

netic field cannot be excited.

From the form of the wave function in Eq. (2), we immediately obtain the selection rules

$$k_x=k_x' \ , \quad z_0=z_0' \ , \tag{10}$$

the latter being equivalent to the conservation of the momentum $\hbar k_y$. Therefore, we have vertical transitions in the surface band structure. The matrix elements for parallel (M^y) and perpendicular excitation (M^z) are derived in Appendix B:

$$M^y_{ii'}=2\left[\frac{d\nu_i}{d\zeta}\frac{d\nu_i'}{d\zeta}\right]^{1/2}\frac{1}{(\nu_i-\nu_i')^2-1} \ , \tag{11a}$$

$$M^z_{ii'}=(\nu_i'-\nu_i)M^y_{ii'} \ . \tag{11b}$$

The matrix elements are normalized with the matrix element of bulk cyclotron resonance between the ground and first excited Landau level. The derivatives in Eqs. (11a) and (11b) are obtained from the zeros of the parabolic cylinder functions (see Appendix A) and are taken at the center coordinate. It is interesting to note, that the matrix elements only depend on the normalized center coordinate z_0/l. Therefore, optical transitions for surface electrons in crossed fields can universally be calculated. The result is shown in Fig. 3, where the transition strengths, i.e., squared matrix elements, are given.

For parallel excitation [Fig. 3(a)], electrons with positive center coordinates ($z_0/l \to \infty$) show the highest excitation strengths, namely those of bulk cyclotron resonance: ($i+1$). No harmonics of CR are allowed in this limit. Through the influence of the surface, harmonics become allowed for center coordinates $z_0/l \approx 0$. For negative center coordinates all transition matrix elements vanish. This is because the corresponding states represent electrons that are strongly bound perpendicular to the surface in the z direction.

The excitation strengths for perpendicular excitation are shown in Fig. 3(b). Unlike for parallel excitation, for more negative center coordinates the transition strengths increase and transitions between, e.g., the ground subband ($i=0$) and higher subbands ($i=2$) become relatively strong.

Summarizing the general results for crossed fields, we realize that the center coordinate is the most important quantum number. Both, hybrid subband energies and transition strengths can analytically and universally be

calculated as a function of this quantum number. From an inspection of Fig. 2 it becomes clear that the parameter $k_D l$ determines the center coordinates that are occupied at a given Fermi energy. This way it also determines the possible excitations in a particular surface band structure.

2. Electric and magnetic limit

In the electric limit ($k_D l \gg +1$) only states with negative center coordinates $z_0/l \ll -1$ are occupied at reasonably low Fermi energies (see Fig. 4). For such center coordinates we obtain the subband energies from Eq. (A1):

$$E \simeq E_{2D} + \left[\frac{9\pi^2}{8m^*}\right]^{1/3} (-\hbar k_y \hbar\omega_c + \hbar e F_s)^{2/3} (i+\tfrac{3}{4})^{2/3} . \tag{12}$$

This equation also describes purely electric subbands[31] ($\hbar\omega_c = 0$) or purely magnetic subbands on metals[2] ($F_s = 0$, $z_0/l \ll -1$). For nearly electric subbands ($k_y \hbar\omega_c \ll eF_s$, i.e., Coulomb force exceeds Lorentz force), the subband dispersion is nearly parabolic, slightly anisotropic with respect to the wave numbers k_x and k_y, and there is a small diamagnetic shift.[8] The anisotropy can be expressed by an effective mass m_y that is obtained from a Taylor expansion of Eq. (12). From this, the density of states

$$D(E) = \sqrt{m_x m_y}/\pi\hbar^2$$

in the electric limit is obtained:

$$D(E) \simeq \frac{m^*}{\pi\hbar^2}\left[1 + \frac{1}{6}\left[\frac{\pi^2}{3}\right]^{1/3} (i+\tfrac{3}{4})^{2/3} (k_D l)^{-4/3}\right] . \tag{13}$$

Note that the density of states increases with subband index i and with smaller $k_D l$ parameters.

The transition strengths in the electric limit can be calculated in closed form. The matrix elements M^y for parallel excitation are zero as can be seen from Fig. 3(a).

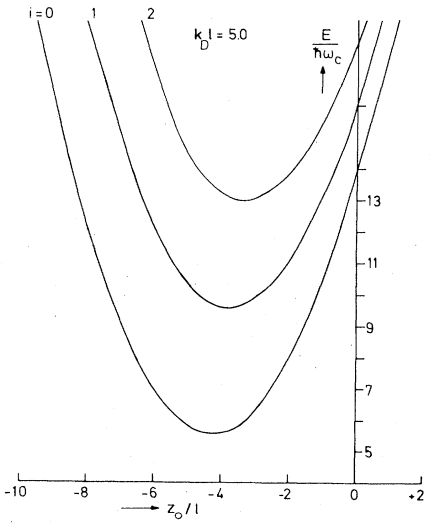

FIG. 4. Surface band structure ($i = 0, 1, 2$) in the electric limit ($k_D l \gg 1$). Cyclotron resonance only is possible for positive center coordinates $z_0/l \gtrsim +1$.

This means, that in the absence of magnetic fields only perpendicular excitation is possible. With Eq. (A1) we obtain

$$M^z_{ii'} = A_0 \frac{e^2\hbar F_s}{m^*}(E_i' - E_i)^{-1} , \tag{14}$$

the energies E_i given by Eq. (12) ($\hbar\omega_c = 0$). The above formula gives the matrix elements for electric intersubband resonance in the approximation of the triangular potential. Since the transition energies $E_i' - E_i$ are proportional to $F_s^{2/3}$, the transition strengths also are proportional to $F_s^{2/3}$.

In the magnetic limit ($k_D l \ll +1$) and at low Fermi energies ($E_F \lesssim \hbar\omega_c$) only positive center coordinates are occupied (see Fig. 5). Then all electrons show bulk behavior and their energy spectrum is given by[35]

$$E \simeq \frac{\hbar^2 k_x^2}{2m^*} + (i+\tfrac{1}{2})\hbar\omega_c + eF_s z_0 + \tfrac{1}{2} m^* v_D^2 . \tag{15}$$

In this limit, the density of states is approximately

$$D(E) \sim \frac{m^*}{\pi\hbar^2}\left[\frac{2E}{\hbar\omega_c}\right]^{1/2} \frac{1}{k_D l} . \tag{16}$$

The optical transitions in the magnetic limit are cyclotron resonances.

3. Various semiconductors

The parameter $k_D l$ characterizes the coupling of the electric and magnetic quantization in crossed fields. It can be tuned by the fields to some extent. In metal-oxide-semiconductor (MOS) structures, the electric field strength is limited by the breakdown field of the gate insulator ($\lesssim 10^{+7}$ V cm^{-1}) and by a minimum field $F_s \sim e n_s/\epsilon_0\kappa_s$ (κ_s static dielectric constant of the semiconductor), for which a sufficiently high electron concentration n_s is obtained. Due to surface trap states and intensity problems, electron densities less than about 10^{11} cm^{-2} can hardly be studied experimentally.[6]

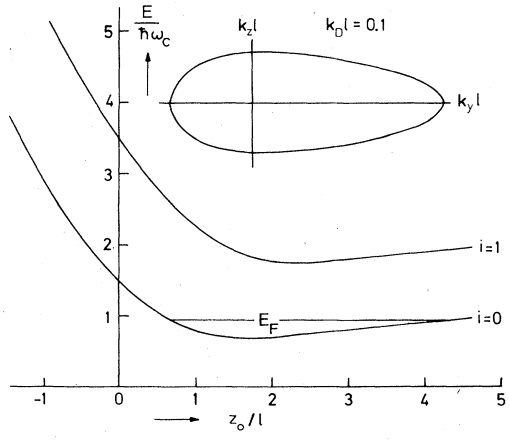

FIG. 5. Surface band structure ($i = 0, 1$) in the magnetic limit ($k_D l \ll 1$). The inset shows the Fermi line for $E_F = \frac{1}{4}\hbar\omega_c$. Cyclotron resonance is possible for most of the center coordinates.

TABLE I. Coupling parameter $k_D l$ for various semiconductors. Density is assumed to be $n_s = 5 \times 10^{11}$ cm^{-2}. Eventual depletion fields are neglected and the transverse effective mass is taken.

	κ_s	m_t^*	$k_D l$ $B=1$ T	5 T	10 T
Si[a]	11.7	0.190	319	29	10
InAs[b]	14.6	0.026	35	3.1	1.1
InSb	17.9	0.014	15	1.1	0.49
$Hg_{1-x}Cd_xTe$[c] ($x \simeq 0.2$)	18.1	0.005	5.4	0.49	0.17
PbTe[d]	400	0.021	1.0	0.09	0.03

[a]Beinvogl *et al.* (Ref. 11).
[b]Maan (Ref. 36).
[c]Zhao *et al.* (Ref. 14).
[d]Schaber and Doezema (Ref. 13).

Table I compares the coupling parameter $k_D l$ on various semiconductors. By this, the experimental findings can qualitatively be understood. In Si, the magnetic field causes only a small shift of the electric intersubband resonance that can be treated in a perturbation approach.[11,12] In narrow-band-gap semiconductors, strong coupling occurs due to their small effective masses. Mixing of the electric and magnetic quantization was observed in the conductivity[7] and in cyclotron resonance[9,36] on InAs and InSb.[10] In corresponding studies on HgCdTe (Refs. 14 and 15) typical laboratory magnetic fields (1–10 T) dominated the electric field and it was suggested that this system be considered in the high-magnetic-field limit.[15] In inversion layers on PbTe,[13] the magnetic limit is definitively realized and bulklike cyclotron resonance was observed. This is mainly due to the large dielectric constant of this material.

Because screening of the electric field is not included in our model, the coupling parameter overestimates somewhat the influence of the electric field if it is calculated by $F_s = e(n_s + N_{\text{depl}})/\kappa_s \epsilon_0$ (N_{depl} denotes depletion charge). Especially at higher electric fields, screening becomes important and one must mimic this effect by a properly chosen effective electric field strength.[30]

C. Two-level model

Table I demonstrates that strong coupling of the electric and magnetic quantization ($k_D l \sim 0.5$) or the magnetic limit ($k_d l \ll 1$) is only observable on narrow-band-gap semiconductors with small effective masses. In order to describe the narrow-band-gap nature of such semiconductors we employ $\mathbf{k}\cdot\mathbf{p}$ perturbation theory in a two-level model.[19,37] As in the one-band model we do not consider the problems of self-consistency of the electrostatic potential but again approximate it by a triangular well potential. Also we neglect effects of spin and spin-orbit interaction. By this, we do not claim that these effects are of minor importance on semiconductors like InSb. The simplified theory, however, allows easy evaluation and interpretation of the experimental results that most prominently reflect nonparabolic effects. Effects of spin are studied in Ref. 30. We start from the effective Schrödinger equation[19]

$$\left\{ -\frac{\hbar^2}{2m_0^*}\frac{\partial^2}{\partial z^2} - \alpha z + \frac{m_0^*}{2}\left[\left[\frac{eB}{m_0^*} \right]^2 - \frac{2e^2 F_s}{m_0^* \epsilon_g} \right] z^2 \right\} \phi = \lambda \phi \ , \tag{17}$$

with $\alpha = \hbar\omega_c k_y - 2eF_s E/\epsilon_g$, $\omega_c = eB/m_0^*$ the cyclotron frequency,

$$\lambda = E^2/\epsilon_g - \epsilon_g/4 - \hbar^2(k_x^2 + k_y^2)/2m_0^* \ ,$$

m_0^* the band-edge mass, and E the energy eigenvalue. We have omitted a term in the effective Hamiltonian that is responsible for Zener interband tunneling.[19,20] It only becomes important in strong electric fields and only when the gap energy is very small.

In solving Schrödinger's equation we must distinguish two cases that mathematically correspond to the two standard differential equations of the parabolic cylinder functions.[34] The two cases are realized for a positive and a negative coefficient in front of the z^2 term in Eq. (17). If an effective cyclotron frequency $\omega_c(1-\delta^2)^{1/2}$ with

$$\delta = \left[\frac{F_s}{B} \right] \left[\frac{2m_0^*}{\epsilon_g} \right]^{1/2} = k_D l \left[\frac{2\hbar\omega_c}{\epsilon_g} \right]^{1/2} \tag{18}$$

is introduced, the two cases are described by $\delta \lesssim 1$, respectively. Note that the parameter δ is the ratio of the drift velocity and the limiting velocity $u = (\epsilon_g/2m_0^*)^{1/2}$ of a semiconductor in the two-level model.[19] In the bulk of semiconductors and in weak electric fields ($\delta < 1$) the eigenfunctions are bound ones and quantization similar to that of the harmonic oscillator is obtained. In strong electric fields ($\delta > 1$) a continuous spectrum is obtained in the bulk whereas in space-charge layers discrete electric subbands near the semiconductor surface form.

With regard to the present experiments, we discuss here the bulklike electrons ($z_0/l \gg +1$, $\delta \leq 1$). Their energy eigenvalues are obtained by completing the square in Eq. (17) and carrying out the usual harmonic oscillator quantization:

$$E_i(k_x,k_y) = (1-\delta^2)^{1/2} \left[\left[\frac{\epsilon_g}{2} \right]^2 + \epsilon_g \left[\hbar\omega_c(1-\delta^2)^{1/2}(i+\tfrac{1}{2}) + \frac{\hbar^2 k_x^2}{2m_0^*} \right] \right]^{1/2} + v_D \hbar k_y \ . \tag{19}$$

When the electric field vanishes ($\delta=0$) the usual result of the two-level model for bulk Landau levels[38] is obtained

$$E_i(k_x)=\left[\left(\frac{\varepsilon_g}{2}\right)^2+\varepsilon_g\left(\hbar\omega_c(i+\tfrac{1}{2})+\frac{\hbar^2k_x^2}{2m_0^*}\right)\right]^{1/2}. \quad (20)$$

The result of the one-band model [Eq. (15)] is recovered in the limit $\varepsilon_g/\hbar\omega_c \ll 1$ and $\delta \ll 1$. It is interesting to note that, unlike in the one-band approximation, the center coordinate and the wave number k_y are no longer strictly proportional:

$$z_0/l=\frac{1}{1-\delta^2}\left[k_y l-\left(\frac{2E}{\varepsilon_g}\right)k_D l\right]. \quad (21)$$

To clarify the physical difference between the one-band and two-level models, let us consider an electron with momentum $\hbar k_y \gg \hbar k_D$. Classically, the trajectory of this electron lies entirely in the interior of the semiconductor (see Fig. 1) and its motion is of magnetic type. Quantum mechanically, the situation is similar in the one-band model: the wave function does almost not feel the influence of the surface and the cyclotron energy is not affected by the electric field. The two-level model gives the physically more meaningful result that in strong electric fields the motion becomes more of electric type, even for bulk electrons. This is expressed by the two factors $(1-\delta^2)^{1/2}$ in Eq. (19): The Landau levels are destroyed when $\delta \to 1$. This is in striking analogy to the behavior of relativistic electrons in free space, as has previously been pointed out.[30]

The transition to an electric type of motion is also indicated by the factor $2E/\varepsilon_g \geq 1$ in Eq. (21) in front of the $k_D l$ parameter. It shifts the center coordinate to more negative values, i.e., quantization into electric subbands is more readily obtained in the two-level approach.

III. EXPERIMENTAL DETAILS

Our samples are metal-oxide-semiconductor (MOS) structures on p-type ($N_A \approx 3\times10^{14}$ cm^{-3}) InSb(111). The InSb substrates were mechanically polished with alumina powder (15—1.0 μm) and subsequently etched in a bromine in methanol ($\approx$0.005%) solution. Then SiO_2 gate insulators ($d \approx 200$ nm) were deposited by a plasma-enhanced chemical-vapor-deposition (CVD) process.[39] As gate contacts semitransparent ($d \approx 3$ nm) NiCr films were evaporated to enable far-infrared transmission experiments.

The onset of inversion was determined from the high-frequency conductivity threshold V_T. The density of inversion electrons

$$n_s=C(V_G-V_T)/eA$$

was calculated from the capacitance C, the gate area ($A \approx 8$ mm^{+2}), and the gate voltage V_G. The density determined this way could be verified within $\pm5\%$ by Shubnikov—de Haas analysis[6] of the quasistatic conductivity.[40] In our spectra, the change of far-infrared transmission caused by the inversion electrons, $\Delta T=T(V_G)-T(V_T)$, is given. In the low-signal limit ($-\Delta T/T \ll 1$), this change is proportional to the high-frequency conductivity of inversion carriers.[41]

The experiments were performed with an optically pumped far-infrared laser and with a Fourier spectrometer.[42] In the laser experiments the magnetic field was swept at fixed inversion electron densities n_s to obtain resonance with the laser energy; in the Fourier spectrometer the magnetic field and the inversion electron density are kept constant. In all experiments, the light vector of the incident radiation was perpendicular to the surface; in some experiments the light was polarized (see Fig. 7). The magnetic field was applied parallel to the surface, thus defining a Voigt configuration.

IV. EXPERIMENTS AND DISCUSSION

A. General features

The most characteristic features of magneto-optical spectra of surface electrons in Voigt configuration can qualitatively be understood in terms of the one-band model in Sec. II B. At low inversion electron densities, when only the lowest hybrid subband and spin level is occupied, effects of nonparabolicity and spin are not very important and the one-band model is applicable to a good approximation.

Figure 6 shows experimental spectra at various infrared laser energies for such a low density ($n_s=3\times10^{11}$ cm^{-2}). The most prominent structure is an absorption maximum that becomes stronger when the laser energy $\hbar\omega$ is increased. The maximum is caused by cyclotron resonance of bulklike electrons in the hybrid subband structure. With increasing laser energy ($\hbar\omega=7.6$—26.6 meV), cyclotron resonance is obtained at higher resonance magnetic fields ($B=1.25$—3.68 T). Correspondingly, the parameter $k_D l$ at cyclotron resonance decreases since the surface

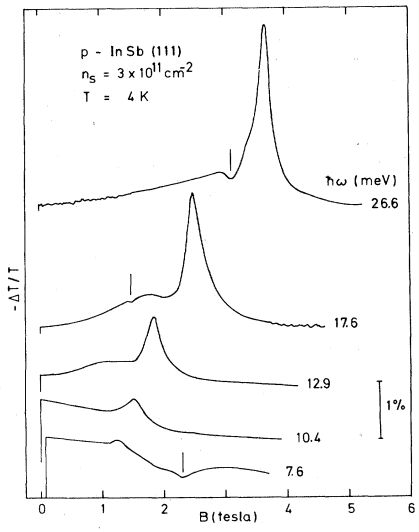

FIG. 6. Experimental spectra of inversion electrons in parallel magnetic fields at various laser energies $\hbar\omega$. The traces have been successively displaced upward. The dashes mark cyclotron resonance of bound holes in the p-type InSb substrate.

electric field $F_s \simeq en_s/\epsilon_0\kappa_s$ is constant at a fixed inversion electron density. Simultaneously, there is a change from a more electric to a more magnetic type of surface band structure (see Fig. 2) and more electrons can contribute to cyclotron resonance. With the band-edge mass $m_0^* = 0.0138$ of InSb we obtain values $k_D l = 7.3$–1.4 from Eqs. (3) and (8).

Assuming Lorentzian line shapes for cyclotron resonance, we can estimate the number of bulklike electrons from the measured change in transmission $\Delta T/T$. The number increases from about 1.2–11 % of the totally induced electrons ($n_s = 3\times 10^{11}\text{cm}^{-2}$). This means that in the trace with the lowest resonance magnetic field ($\hbar\omega = 7.6$ meV) cyclotron resonance of only about 4×10^9 cm^{-2} electrons is detected. The increase of the number of electrons is in qualitative agreement with theory. However, for the laser energy $\hbar\omega = 7.6$ meV, i.e., resonance magnetic field $B = 1.25$ T, no bulklike electrons are expected when the hybrid subbands and the Fermi energy are calculated according to Eqs. (9) and (13), respectively. We think that, due to screening effects, the effective parameter $k_D l$ is lower than $k_D l = 7.3$ and still few subband states with center coordinates $z_0/l \gtrsim 1$ are occupied.

For the energy, e.g., $\hbar\omega = 26.6$ meV, the most positive center coordinates lie about two cyclotron radii inside the semiconductor and we expect that 7% of the induced electrons contribute to cyclotron resonance. The experimental value is 11%. Better agreement can be obtained (for all laser energies) if screening is mimicked by an effective surface electric field $F_{\text{eff}} \approx \frac{1}{2}F_s$.

There is also background absorption in the spectra of Fig. 6 that changes with laser energy. At low laser energies, the background slightly decreases with magnetic field. We interpret this as intraband absorption of Drude electrons. As is expected, Drude absorption at zero magnetic field strongly decreases with increasing laser energy. In addition to Drude absorption, a broad background resonance is observed. It is most clearly present in the traces for the energies $\hbar\omega = 12.9$ and 17.6 meV. This broad absorption is caused by transitions different from cyclotron resonance between the ground and the first excited hybrid subband, i.e., it is caused by electrons with center coordinates $z_0/l \lesssim 1$. The transition energies of these electrons depend on their center coordinates (see Fig. 4) causing broad structures. The background is much weaker than cyclotron resonance since the corresponding excitation strengths ($z_0/l \lesssim +1$) are weaker in parallel excitation [see Fig. 3(a)] and the joint density of states is less than for the parallel hybrid subbands at $z_0/l \gtrsim +1$. The dashes in Fig. 6 indicate cyclotron resonance of bound holes in the p-type substrate (cf. Ref. 43).

Figure 7 compares cyclotron resonance of inversion electrons in the Voigt and Faraday configurations with cyclotron resonance in a bulk sample of n-type InSb (inset of Fig. 7). The figure also demonstrates the dependence on the polarization of the incident light. Cyclotron resonance in the bulk sample ($d = 110\ \mu$m) was found to be identical in the Voigt and Faraday configurations, as is expected for the low density ($n = 6\times 10^{13}$ cm^{-3} at 77 K). Due to magnetic freeze-out at liquid-helium temperature,[44] the majority of electrons shows impurity shifted cyclotron resonance ($B = 6.7$ T); only few electrons show conduction-band cyclotron resonance ($B = 6.9$ T, cf. Ref. 45).

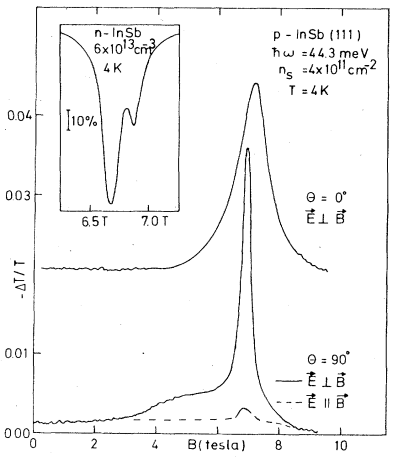

FIG. 7. Comparison of bulk cyclotron resonance (conduction-band and impurity-shifted resonances) in n-type InSb (inset) with surface cyclotron resonance in inversion layers on p-type InSb. Surface cyclotron resonance is shown for the Faraday configuration ($\theta = 0°$) and Voigt configurations ($\theta = 90°$). The light vector is always perpendicular to the surface ($\mathbf{k}\perp S$). In the Voigt configuration ($\mathbf{k}\perp\mathbf{B}$) the light can be polarized parallel ($\mathbf{E}||\mathbf{B}$) or perpendicular ($\mathbf{E}\perp\mathbf{B}$) to the magnetic field.

The resonance position in inversion layers in Voigt configuration is nearly the same as for conduction-band electrons in the bulk sample. This provides the strongest experimental evidence that we actually observe bulklike cyclotron resonance in inversion layers in parallel magnetic fields. The resonance magnetic field of inversion electrons in Faraday configuration $B = 7.25$ T is slightly higher than in Voigt configuration. This is due to different nonparabolic effects in both configurations.[40]

The mobility of inversion electrons that can be deduced from the linewidth is higher in Voigt configuration ($\mu \simeq 6.7\times 10^{+4}$ cm^{+2}V^{-1}s^{-1}) than in Faraday configuration ($\mu \simeq 1.5\times 10^{+4}$ cm^{+2}V^{-1}s^{-1}). This can be explained by reduced effects of surface scattering due to interface charges and surface roughness. The center coordinates of bulklike electrons lie far inside the semiconductor ($z_0/l \simeq 2$–$3, l = 95$ Å) in Voigt configuration, whereas the envelope function in Faraday configuration has an average distance of about 150 Å from the surface.[6,32] The mobility in the bulk sample is still higher: $\mu \simeq 20\times 10^{+4}$ cm^{+2}V^{-1}s^{-1}.

The dependence on polarization of the incident light is also demonstrated in Fig. 7. Since the light always impinges in the direction perpendicular to the sample in the present experiments, the light is polarized perpendicular to the magnetic field in Faraday configuration ($\theta = 0°$, $\mathbf{E}\perp\mathbf{B}$). In Voigt configuration, the polarization can either be parallel to the magnetic field ($\mathbf{E}||\mathbf{B}$) or perpendicular to it ($\mathbf{E}\perp\mathbf{B}$). Cyclotron resonance is only significantly presented in the perpendicular polarization, as is expected

from the discussion in Sec. II B. The small structure that is left in parallel polarization (dashed line) is probably due to imperfect polarization. Interband transitions different from cyclotron resonance have an onset at about $B \simeq 3$ T and are only present measurably when the light is polarized perpendicular to the magnetic field (see Sec. II B 1). In contrast to this, the Drude background does not significantly depend on polarization.

B. Cyclotron resonance

We now discuss in more detail experimental results of cyclotron resonance at various laser energies. As was explained above, higher laser energies yield higher resonance magnetic fields and lower parameters $k_D l$. In the experiments, the surface electric field is proportional to the electron density only just inside the semiconductor and only if the depletion field is neglected. Since in our model self-consistency was not considered, we do not know exactly the effective electric field at center coordinates in the interior of the semiconductor. Therefore, we will give resonance magnetic fields as a function of the measured inversion electron density n_s.

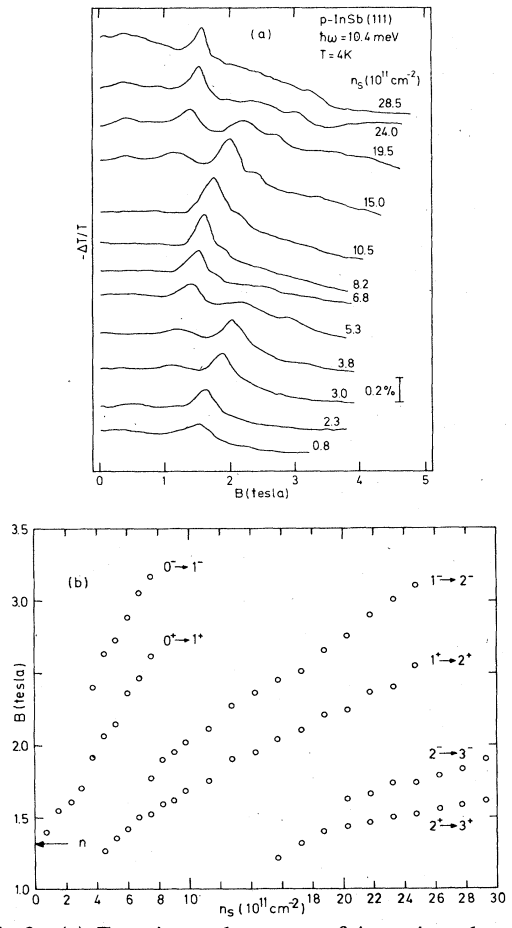

FIG. 8. (a) Experimental spectra of inversion electrons in parallel magnetic fields at the laser energy $\hbar\omega = 10.4$ meV. The traces have successively been displaced upward for clarity. (b) Resonance magnetic fields versus inversion electron density n_s. The arrow gives the bulk value in n-type InSb.

Figure 8(a) shows representative spectra for a low laser energy. These spectra are dominated by Drude absorption; only a few electrons contribute to cyclotron resonance. At low densities ($n_s \lesssim 4\times10^{11}$ cm^{-2}) only one cyclotron maximum is present. When the density is increased, it shifts to higher magnetic fields and a shoulder evolves on its high-field side. The shift is caused by nonparabolicity (see Sec. II C), the splitting by spin-up and spin-down transitions ($0^{\pm}\rightarrow1^{\pm}$). At higher densities the maxima broaden and disappear at densities $n_s \gtrsim 8\times10^{11}$ cm^{-2}. A second maximum ($1^{\pm}\rightarrow2^{\pm}$) evolves at densities $n_s \gtrsim 4\times10^{11}$ cm^{-2} roughly at the position where the first transition started. This maximum also shifts to higher magnetic fields, splits, and broadens at higher densities. The situation repeats with a third maximum ($2^{\pm}\rightarrow3^{\pm}$).

In the one-band model (see Fig. 4) cyclotron resonance $i'\rightarrow i'+1$ is expected for all subbands $i' \leq i$, when cyclotron transitions $i\rightarrow i+1$ are observed. Since in lower subbands cyclotron resonance takes place at more positive center coordinates, we expect sharper lines in lower subbands due to reduced scattering by interface impurities and surface roughness.

However, contrary to this prediction of the one-band model, the transitions, e.g., $0^{\pm}\rightarrow1^{\pm}$, broaden and disappear at higher densities. This has recently[30] been explained with the two-level model. According to Eq. (19), there is a destruction of the Landau quantization in crossed electric and magnetic fields ($\delta\rightarrow1$). If no screening of the electric field is considered and if the depletion field is neglected, i.e., $F_s = en_s/\epsilon_0\kappa_s$ is assumed, the situation $\delta = 1$ should be reached at $n_s \simeq 2.5\times10^{11}$ cm^{-2}, whereas it is experimentally observed at $n_s \simeq 6\times10^{11}$ cm^{-2}. This discrepancy is presumably due to screening of the electric field and the factor of about 2 agrees with the one found above.

Also, in the triangular-well approximation (F_s constant) all cyclotron transitions $i\rightarrow i+1$ should disappear simulataneously when $\delta\rightarrow1$. This is evidently not the case in Fig. 8(a) and may also be explained by a more realistic electric surface potential. Real behavior in a MOS structure is sublinear, so that higher magnetic states are subjected to weaker electric fields, which qualitatively agrees with the observations.

From the experimental spectra, resonance magnetic fields were extracted. They are shown in Fig. 8(b) versus electron density. At a low occupancy of a particular hybrid subband, the resonance field is nearly identical with the one in n-type InSb with a low-volume electron concentration, i.e., the effective surface electric field is very small. In the limit $n_s\rightarrow0$ the position is the one of bulk cyclotron resonance and also the spin splitting agrees with the bulk value (cf. Ref. 45).

It is interesting to compare the onset of occupation of higher hybrid subbands with the onset in purely electric subbands.[40] If the transitions $i^+\rightarrow(i+1)^+$ are extrapolated to the resonance field of n-type InSb ($B = 1.32$ T), we obtain subband thresholds $n_1 \simeq 4\times10^{11}$ cm^{-2} and $n_2 \sim 16\times10^{11}$ cm^{-2}. These values are higher than in purely electric subbands ($n_1 \sim 2\times10^{11}$ cm^{-2}, $n_2 \sim 4\times10^{11}$

cm^{-2}). This is a consequence of the enhanced density of states in a parallel magnetic field [see Eq. (13)].

Figure 9(a) shows representative spectra for a higher transition energy, i.e., for higher resonance magnetic fields. The resonances are more pronounced as was already discussed with the aid of Fig. 6. There is always a cyclotron-resonance maximum near the resonance field of n-type InSb ($B=2.34$ T). Out of the maximum various other maxima are successively split off when the density is increased.

In Fig. 9(b) these split-off maxima are assigned to spin-up and spin-down cyclotron resonances $0^{\pm}\rightarrow 1^{\pm}$ and $1^{\pm}\rightarrow 2^{\pm}$. We think that the maximum at $B\simeq 2.3$ T (solid circles) is caused by small occupancies of correspondingly higher subbands. This means that at densities $3\times 10^{11}\lesssim n_s\lesssim 10\times 10^{11}$ cm^{-2} it represents transitions $1^{\pm}\rightarrow 2^{\pm}$, and at densities $n_s\gtrsim 10\times 10^{11}$ cm^{-2} transitions $2^{\pm}\rightarrow 3^{\pm}$. This interpretation is supported by a small but discernible dependence of the resonance field on electron density. Again, this demonstrates that cyclotron resonance in each particular hybrid subband starts at the same position, namely at vanishing effective-field strength F_s.

Below the cyclotron-resonance fields additional structures are observed. They are marked by arrows in Fig. 9(a). By comparison of their resonant magnetic fields ($n_s\rightarrow 0$) with n-type InSb ($B=1.7$ T), we conclude that they are harmonic cyclotron resonances. They are most clearly observed at the laser energy $\hbar\omega=17.6$ meV, presumably because of the relatively high $\omega\tau$ values obtained at this energy.

There are two mechanisms by which harmonic cyclotron resonance can be induced: the influence of the surface [see Fig. 3(a)] and the breakdown of selection rules as it is predicted from the two-level model in crossed electric and magnetic fields in the bulk.[46] Since in the present experiments mostly three-dimensional electrons are ob-

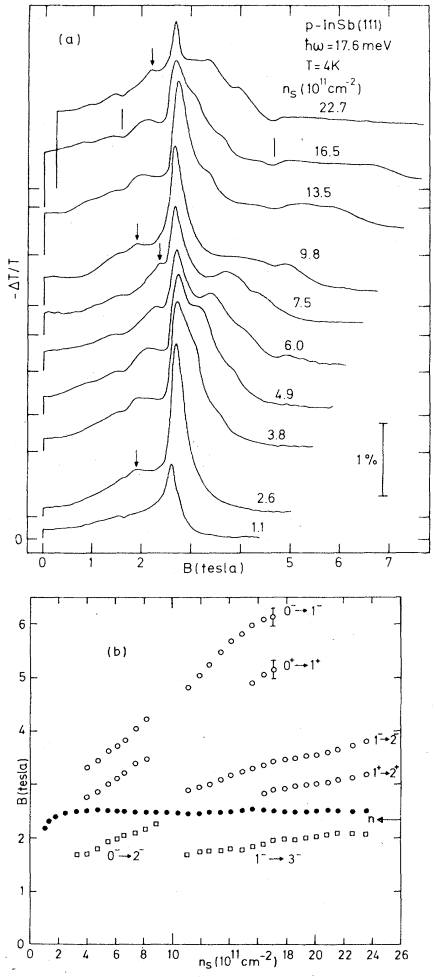

FIG. 9. (a) Experimental spectra of inversion electrons in parallel magnetic fields at the laser energy $\hbar\omega=17.6$ meV. The horizontal lines at $B=0$ successively mark the value $-\Delta T/T=0$. The arrows indicate harmonic cyclotron resonances, the dashes cyclotron resonances of bound holes in the p-type substrate. (b) Resonance magnetic fields vs inversion electron density n_s. The solid dots represent cyclotron resonances in higher hybrid subbands. The arrow gives the bulk value in n-type InSb.

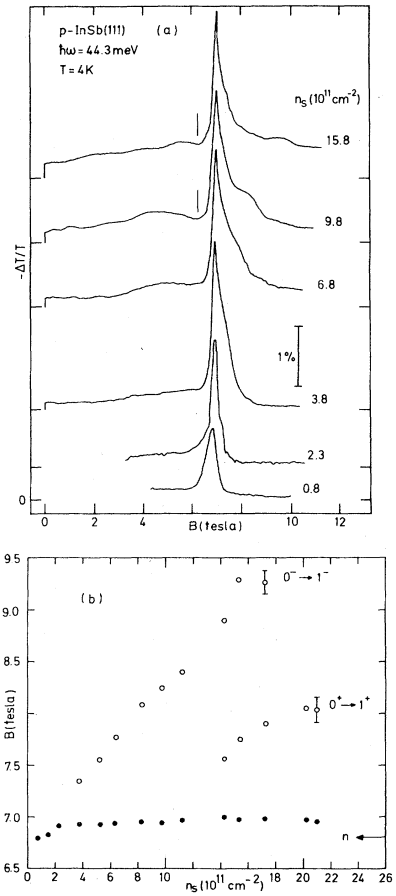

FIG. 10. (a) Experimental spectra of inversion electrons in parallel magnetic fields at the laser energy $\hbar\omega=44.3$ meV. The horizontal lines successively mark the value $-\Delta T/T=0$. The dashes indicate cyclotron resonances of bound holes in the p-type substrate. (b) Resonance magnetic fields versus inversion electron density n_s. The solid circles represent cyclotron resonances in higher hybrid subbands. The arrow gives the bulk value in n-type InSb.

served, the second mechanism seems to be more important.

Figure 10(a) shows representative spectra for a still higher transition energy. The Drude background now is drastically reduced and the spectra are dominated by a strong cyclotron resonance. The resonance magnetic field of the prominent maximum [Fig. 10(b)] is nearly identical with the one in n-type InSb ($B=6.81\pm0.01$ T) but slightly increases with density up to $B=7.01$ T at $n_s\simeq15\times10^{11}$ cm^{-2}. Then it decreases down to magnetic fields $B=6.95$ T at $n_s=21\times10^{11}$ cm^{-2}. From this dominant maximum two shoulders are successively split off. We interpret these as transitions $0^+\rightarrow1^+$ and $0^-\rightarrow1^-$, respectively. The dominant cyclotron maximum is caused by cyclotron resonance of the ground hybrid subband at low densities ($n_s\lesssim5\times10^{11}$ cm^2) but by cyclotron resonance $1^\pm\rightarrow2^\pm$ at higher densities.

The number of hybrid subbands occupied in the density range $n_s\lesssim15\times10^{11}$ cm^{-2} reduces from three to one when the laser energy is increased from $\hbar\omega=10.4$—44.3 meV. This can qualitatively be explained by the density of states given in Eq. (13): at higher resonance magnetic fields, i.e., lower parameters k_Dl, the density of states in a particular hybrid subband is higher and fewer subbands are occupied at the same density.

In Fig. 11 experimental cyclotron masses $m^*=eB/\omega$ for the $0^+\rightarrow1^+$ transition are depicted for two densities n_s. Also the experimental values of an n-type sample are included.

The data of the n-type sample (bulk conduction-band cyclotron resonance) can only be described with Eq. (20), if an effective band-gap energy $\varepsilon_g=0.33$ eV is assumed. This effective band-gap energy compensates for the neglected spin-orbit interaction[30] and Eq. (20) describes the experimental results quite well above and below the reststrahlen band. For the theoretical curves of the inversion electrons in Fig. 11 surface electric fields must be assumed that are a factor of 2 lower than the unscreened fields $F_s=en_s/\epsilon_0\kappa_s$. Such a factor was already found above when the number of electrons contributing to cyclotron resonance and when the effective electric field entering δ in Eq. (18) were considered.

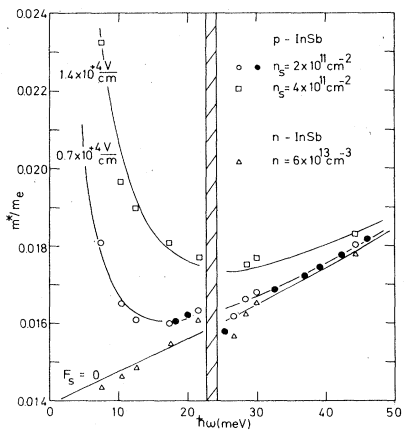

FIG. 11. Electron-cyclotron masses in InSb ($0^+\rightarrow1^+$). Experimental data were obtained by laser (open symbols) and Fourier spectroscopy ($n_s=2\times10^{11}$ cm^{-2}, solid circles). Cyclotron masses of inversion electrons in parallel magnetic fields (crossed-field configuration) are given for two inversion electron densities n_s. For comparison, bulk masses of n-type InSb are included. Solid lines are calculated from the two-level model. The hatched region indicates the reststrahlen band.

C. Polarons

The electron-phonon interaction in polar semiconductors manifests itself through collective and single-particle effects, i.e., polarons.[47] The latter is addressed as resonant magnetopolaron, when the cyclotron energy approximately equals the LO-phonon energy ($\hbar\omega_c\simeq\hbar\omega_{LO}$). In this nearly resonant situation, the cyclotron mass is increased below the the reststrahlen band and is decreased above it, compared with the nonparabolic mass alone (see Fig. 11 for $F_s=0$ and $F_s=0.7\times10^{+4}$ V cm^{-1}). Polarons are not studied for the density $n_s=4\times10^{11}$ cm^{-2}, because the $0^+\rightarrow1^+$ transition could not be resolved with sufficient accuracy at this density.

It is astonishing that resonant polarons are observed in a degenerate system in Voigt configuration, since in thin slabs of highly doped n-type InSb collective plasma cyclotron—LO-phonon modes are observed[23] that totally mask the polaron effect.

Two recent theories deal with plasma shifts in inversion layers in the Voigt configuration. In the theory of Chaplik and Magarill[48] it is shown in a perturbation approach, that the plasma shift is compensated by the renormalization of the cyclotron frequency in a realistic electric surface potential. Heyszenau[49] found the rigorous result that the electron-electron interaction does not lead to a shift of the resonance positon in the present configuration.

Effects of LO phonons have not yet been included in the above-mentioned theories, but it is clear from the experimental results[25] that no collective plasma—LO-phonon modes exist in the Voigt configuration in inversion layers. Instead of this, single-particle excitations (polarons) are observed near the reststrahlen band.

As an experimental measure of the resonant polaron effect we have taken the mass discontinuity Δm between an energy just below (21.8 meV) and just above (26.6 meV)

TABLE II. Mass discontinuities of resonant surface polarons. Experimental error $1\times10^{-4}m_e$. Bulk polarons do not depend on configuration at low bulk densities n.

Configuration	Density n_s (cm^{-2})	Discontinuity Δm ($10^{-4}m_e$)
Voigt[a]	0.2×10^{12}	3
	1.0×10^{12}	3
Faraday[b]	0.2×10^{12}	11
	1.0×10^{12}	24
Bulk electrons[c]		4
	$n=6\times10^{13}$ cm^{-3}	
Magnetodonors		3.5

[a]Horst and Merkt (Ref. 25).
[b]Horst *et al.* (Ref. 27).
[c]Compare with, e.g., C. J. Summers *et al.*, Phys. Rev. **170**, 755 (1968).

the reststrahlen band.[25] In Table II the resonant polaron is compared with the one in Faraday configuration and with the resonant polaron of conduction-band electrons and magnetodonors in n-type bulk InSb.

The enhanced polaron effect in Faraday configuration has been explained by the form of the wave function[50] that leads to relatively high matrix elements of the polar interaction. This argument does not hold for the present Voigt configuration since the wave functions in this configuration are nearly identical with volume functions. Comparison of resonant Voigt-configuration polarons and volume polarons also indicates that screening of the polar interaction[26] in the present degenerate electron system and influence of interface or two-dimensional (2D) phonons[51] do not seem to be important in inversion layers.

V. SUMMARY

We have studied cyclotron resonance of inversion electrons on InSb in magnetic fields parallel to the surface, when the wave vector of the incident light is perpendicular to the surface. As far as only the magnetic part of the surface potential is considered, this geometry is analogous to the Voigt configuration in volume semiconductors[47] and to the configuration of magnetic surface levels in metals.[1] In inversion layers, a degenerate electron gas near the semiconductor surface is created by the surface electric field and a crossed-field configuration is established.

We have calculated the resulting hybrid electric-magnetic surface band structure and its optical excitations in the one-band effective-mass approximation for a triangular electric potential well. Similar to Voigt configuration in volume semiconductors, transitions between Landau-like levels are the most pronounced excitations of hybrid subbands on semiconductor surfaces. Such cyclotron resonances were studied experimentally in the present paper.

The one-band model successfully describes the transition from a more electric to a more magnetic type of surface band structure, which is observed in the cyclotron-resonance experiments when the magnetic field is increased with respect to the electric field.

The surface electric field influences cyclotron resonance. In weak magnetic fields experimental cyclotron masses strongly increase when the surface electric field, i.e., inversion electron density, is increased. In strong magnetic fields this effect is far less pronounced. This cannot be explained in the one-band model, but can quantitatively be explained with a two-level model that accounts for the nonparabolicity of electrons in crossed electric and magnetic fields. This model may also be useful in describing experimental results on other narrow-band-gap semiconductors, like InAs (Refs. 7, 36) or HgCdTe (Ref. 14).

There are still open questions. In particular, a self-consistent surface potential including spin-orbit interaction is required to describe cyclotron resonance in higher hybrid subbands and the observed spin splitting of cyclotron resonance more quantitiatively.

ACKNOWLEDGMENTS

The author thanks J. P. Kotthaus for continuous encouragement and stimulating discussions, and acknowledges collaboration with W. Zawadzki. Thanks are also due J. H. Crasemann, M. Horst, and S. Klahn. This work was supported by the Deutsche Forschungsgemeinschaft.

APPENDIX A: ZEROS OF PARABOLIC CYLINDER FUNCTIONS

The parabolic cylinder function $D_\nu(\zeta)$ has $[\nu+1]$ zeros, the square brackets denoting the greatest positive integer less than $\nu+1$ (see, e.g., Ref. 52). If the index ν is an integer, D_ν is closely related to the Hermite polynomial H_ν and the zeros are well known.[34,53]

Because the index determines the energy in Eq. (9), the degeneracy of surface Landau levels ($F_s=0$) is given by the number of zeros of the function D_ν. In our scheme, the wave functions of these degenerate states belong to different subbands i and to different center coordinates z_0/l. This is demonstrated in Fig. 12(a) with an example

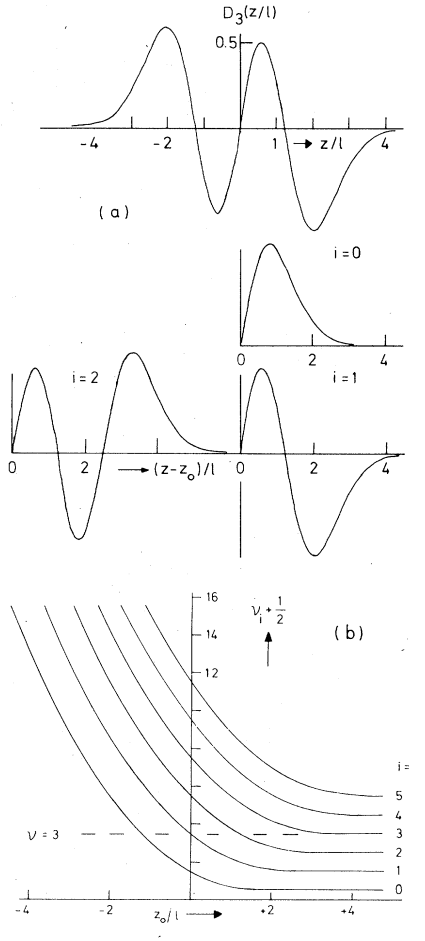

FIG. 12. (a) Construction of eigenfunctions. The boundary condition at the surface $z=0$ is satisfied by taking parts of the parabolic cylinder function, e.g., of D_3. This leads to hybrid subband functions ($i=0,1,2$) for degenerate levels ($E=\frac{7}{2}\hbar\omega_c$) with different center coordinates $z_0/l=0,\pm1.22$. (b) Zeros z_0/l of the parabolic cylinder functions $D_\nu(z)$. The most negative zero for each index ν belongs to the ground subband $i=0$. Correspondingly, higher subbands are obtained.

($\nu=3$). Three eigenfunctions with zeros at the surface $z=0$ can be constructed from D_3. All functions belong to the same energy $\frac{7}{2}\hbar\omega_c$, but to different subbands $i=0,1,2$ and center coordinates z_0/l. Since the index ν was assumed to be an integer, the original function D_3 is an eigenfunction in the limit $z_0/l\to\infty$.

With the zeros in Fig. 12(b), the energy eigenvalues in Eq. (9) and the matrix elements for electric dipole transitions in Eqs. (11a) and (11b) can be determined for arbitrary strengths of the fields. For values not included in the figure, the following approximate formulas can be used:

$$\nu_i\simeq\begin{cases}\frac{1}{2}(z_0/l)^2-\frac{1}{2}+\frac{1}{2}[3\pi(i+\frac{3}{4})]^{2/3}(z_0/l)^{2/3}\ , & z_0/l\ll-1 \\ i+\dfrac{2^i}{i!}\left[\dfrac{1}{\pi}\right]^{1/2}(z_0/l)^{2i+1}e^{-(z_0/l)^2}\ , & z_0/l\gg+1\ .\end{cases} \tag{A1}$$

(A2)

The approximation given in Eq. (A1) corresponds to the semiclassical Bohr-Sommerfeld result for electrons in a triangular potential that has extensively been discussed in connection with magnetic surface levels in metals and semimetals.[1,2] Equation (A2) is due to Kaner, Makarov, and Fuks.[54] We also note an approximation derived by Dean[55] for center coordinates close to the surface. It reads

$$\nu_i\simeq(2i+1)-\left[\frac{4}{\pi}\right]^{1/2}\frac{(2i+1)!!}{(2i)!!}(z_0/l)\ ,\quad z_0/l\approx0 \tag{A3}$$

in its most simple form. In Eq. (A3) we make use of the abbreviations

$$(2i)!!\equiv(2i)\times\cdots\times(2i-2)\times\cdots\times2$$

and

$$(2i+1)!!\equiv(2i+1)\times(2i-1)\times\cdots\times1\ .$$

APPENDIX B: NORMALIZATION AND TRANSITION MATRIX ELEMENTS

Electric dipole matrix elements are calculated for the initial state D_ν, the final state D'_ν, and the perturbation

$$H_{\rm rad}=-(e/m^*)\mathbf{A}'\cdot\mathbf{P}\ ,$$

where $\mathbf{A}'$ is the vector potential of the incident light wave and $\mathbf{P}=\mathbf{p}+e\mathbf{A}$ the kinetic momentum of the surface electron. Taking into account the relation $z_0/l=k_yl-k_Dl$ given in Eq. (5), we obtain [$\zeta=\sqrt{2}(z-z_0)/l$]

$$H^y_{\rm rad}=A'_0\frac{el\omega_c}{\sqrt{2}}\zeta \tag{B1a}$$

and

$$H^z_{\rm rad}=iA'_0\sqrt{2}el\omega_c\frac{\partial}{\partial\zeta} \tag{B1b}$$

for parallel $\mathbf{A}'=(0,A'_0,0)$ and perpendicular excitation $\mathbf{A}'=(0,0,A'_0)$, respectively. The gauge of the static magnetic field is $\mathbf{A}=(0,-Bz,0)$. Since the recurrance relations[34]

$$\frac{dD_\nu}{d\zeta}+\tfrac{1}{2}\zeta D_\nu(\zeta)-\nu D_{\nu-1}=0 \tag{B2a}$$

and

$$D_{\nu+1}-\zeta D_\nu(\zeta)+\nu D_{\nu-1}=0 \tag{B2b}$$

hold, only integrals ($\zeta_0=-\sqrt{2}z_0/l$)

$$\int_{\zeta_0}^{+\infty}D_\mu D_\nu\,d\zeta=\frac{1}{\nu-\mu}D_\mu(\zeta_0)\frac{\partial D_\nu}{\partial\zeta}\bigg|_{\zeta=\zeta_0} \tag{B3}$$

must be calculated for the matrix elements. Note, that D_ν is an eigenstate, but D_μ is not, except if $\zeta_0\to-\infty$. The integral is solved by partial integration of Eq. (7). The normalization integral is obtained from Eq. (B3) in the limit $\mu\to\nu$:

$$\int_{\zeta_0}^{+\infty}D_\nu D_\nu\,d\zeta=-\frac{\partial D_\nu}{\partial\zeta}\frac{dD_\nu}{d\nu}\bigg|_{\zeta=\zeta_0}\ . \tag{B4}$$

If a Taylor expansion with respect to the index ν and the coordinate ζ,

$$D_{\nu+d\nu}(\zeta+d\zeta)=D_\nu(\zeta)+\frac{\partial D_\nu}{\partial\zeta}d\zeta+\frac{\partial D_\nu}{\partial\nu}d\nu\ ,$$

is considered with eigenstates $D_{\nu+d\nu}(\zeta+d\zeta)$ and $D_\nu(\zeta)$,

$$\frac{\partial D_\nu}{\partial\nu}=-\left[\frac{\partial D_\nu}{\partial\zeta}\right]\left[\frac{d\nu}{d\zeta}\right]^{-1}\ . \tag{B5}$$

The derivative is taken with respect to the center coordinate in a particular subband i. The derivatives $d\nu/d\zeta$ can be calculated numerically from the values in Fig. 12(b).

The matrix element for parallel excitation,

$$\langle\nu'\,|\,H^y_{\rm rad}\,|\,\nu\rangle=A'_0\frac{el\omega_c}{\sqrt{2}}\frac{\langle\nu'\,|\,\zeta\,|\,\nu\rangle}{\langle\nu'\,|\,\nu'\rangle^{1/2}\langle\nu\,|\,\nu\rangle^{1/2}}\times\delta_{z_0,z'_0}\delta_{k_x,k'_x}\ ,$$

is obtained from Eqs. (B3)—(B5). It is convenient to normalize it with the matrix element for bulk cyclotron resonance $A'_0el\omega_c/\sqrt{2}$ between the ground and the first excited Landau level. Then Eq. (11a) is obtained. The matrix element for perpendicular excitation is calculated similarly.

For the important case of a surface electron with center coordinate at the surface ($z_0=0$), the matrix elements for transitions $i\to i'$ can be given in the closed form

$$M^y_{ii'}(z_0=0)=\left[\frac{8}{\pi}\right]^{1/2}\left[\frac{(2i+1)!!(2i'+1)!!}{(2i)!!(2i')!!}\right]^{1/2}\times[4(i-i')^2-1]^{-1}\ . \tag{B6}$$

The corresponding matrix element M^z for perpendicular excitation is $M^z=2(i'-i)M^y$.

[1]M. S. Khaikin, Adv. Phys. **18**, 1 (1969).
[2]R. E. Prange and T. W. Nee, Phys. Rev. **168**, 779 (1968).
[3]R. E. Doezema and J. F. Koch, Phys. Rev. B **5**, 3866 (1972).
[4]J. F. Koch and J. D. Jensen, Phys. Rev. **184**, 643 (1969).
[5]M. Wanner, R. E. Doezema, and U. Strom, Phys. Rev. B **12**, 2883 (1975).
[6]T. Ando, A. B. Fowler, and F. Stern, Rev. Mod. Phys. **54**, 437 (1982).
[7]R. E. Doezema, M. Nealon, and S. Whitemore, Phys. Rev. Lett. **45**, 1593 (1980).
[8]F. Koch, in *Physics in High Magnetic Fields,* Proceedings of the Oji International Seminar, Hakone, Japan, 1980, edited by S. Chikazumi and M. Miura (Springer, Berlin, 1981).
[9]J. C. Maan, Ch. Uihlein, L. L. Chang, and L. Esaki, Solid State Commun. **44**, 653 (1982).
[10]J. H. Crasemann, U. Merkt, and J. P. Kotthaus, Phys. Rev. B **28**, 2271 (1983).
[11]W. Beinvogl, A. Kamgar, and J. F. Koch, Phys. Rev. B **14**, 4274 (1976).
[12]T. Ando, Phys. Rev. B **19**, 2106 (1979).
[13]H. Schaber and R. E. Doezema, Phys. Rev. B **20**, 5257 (1979).
[14]W. Zhao, C. Mazurè, F. Koch, J. Ziegler, and H. Maier, Surf. Sci. **142**, 400 (1984).
[15]W. Zhao, F. Koch, J. Ziegler, and H. Maier, Phys. Rev. B **31**, 2416 (1985).
[16]A. G. Aronov, Fiz. Tverd. Tela (Leningrad) **5**, 552 (1963) [Sov. Phys.—Solid State **5**, 402 (1963)].
[17]Q. H. F. Vrehen and B. Lax, Phys. Rev. Lett. **12**, 471 (1964).
[18]Q. H. F. Vrehen, Phys. Rev. **145**, 675 (1966).
[19]W. Zawadzki and B. Lax, Phys. Rev. Lett. **16**, 1001 (1966).
[20]W. Zawadzki, Surf. Sci. **37**, 218 (1973).
[21]M. Reine, Q. H. F. Vrehen, and B. Lax, Phys. Rev. **163**, 726 (1967).
[22]S. Iwasa, Y. Sawada, E. Burstein, and E. D. Palik, in Proceedings of the 8th International Conference on the Physics of Semiconductors, Kyoto, 1966 [J. Phys. Soc. Jpn. Suppl. **21**, 742 (1966)].
[23]R. Kaplan, E. D. Palik, R. F. Wallis, S. Iwasa, E. Burstein, and Y. Sawada, Phys. Rev. Lett. **18**, 159 (1967).
[24]M. Horst, U. Merkt, and J. P. Kotthaus, Solid State Commun. **49**, 707 (1984).
[25]M. Horst and U. Merkt, Solid State Commun. **54**, 559 (1985).
[26]S. Das Sarma, Phys. Rev. B **27**, 2590 (1983).
[27]M. Horst, U. Merkt, and J. P. Kotthaus, Phys. Rev. Lett. **50**, 754 (1983).
[28]J. F. Koch, Surf. Sci. **58**, 104 (1976).
[29]J. D. Jackson, *Classical Electrodynamics,* 2nd ed. (Wiley, New York, 1975), p. 582.
[30]W. Zawadzki, S. Klahn, and U. Merkt, Phys. Rev. Lett. **55**, 983 (1985).
[31]F. Stern, Phys. Rev. B **5**, 4891 (1972).
[32]Y. Takada, K. Arai, N. Uchimura, and Y. Uemura, J. Phys. Soc. Jpn. **49**, 1851 (1980).
[33]Y. Takada, J. Phys. Soc. Jpn. **50**, 1998 (1981).
[34]J. C. P. Miller, in *Handbook of Mathematical Functions,* edited by M. Abramowitz and I. A. Stegun (Dover, New York, 1965), Chap. 19, pp. 685—720.
[35]W. Zawadzki, in *Physics of Solids in Intense Magnetic Fields,* edited by E. D. Haidemenakis (Plenum, New York, 1969), Chap. 14, pp. 311—327.
[36]J. C. Maan, Intern. J. Infrared Millimeter Waves **8**, 387 (1983).
[37]W. Zawadzki, J. Phys. C **16**, 229 (1983).
[38]W. Zawadzki, in *New Developments in Semiconductors,* edited by P. R. Wallace *et al.* (Noordhoff, Leiden, 1973), pp. 441—468.
[39]U. Mackens and U. Merkt, Thin Solid Films **97**, 53 (1982).
[40]U. Merkt, T. Evelbauer, M. Horst, and J. P. Kotthaus (unpublished).
[41]S. J. Allen, Jr., D. C. Tsui, and F. De Rosa, Phys. Rev. Lett. **35**, 1359 (1975).
[42]E. Batke and D. Heitmann, Infrared Phys. **24**, 189 (1984).
[43]C. L. Litter, D. G. Seiler, R. Kaplan, and R. J. Wagner, Phys. Rev. B **27**, 7473 (1983).
[44]A. Raymond, J. L. Robert, W. Zawadzki, and J. Wlasak, J. Phys. C **17**, 2381 (1984).
[45]E. J. Johnson and D. H. Dickey, Phys. Rev. B **1**, 2676 (1970).
[46]W. Zawadzki, in *Proceedings of the 9th International Conference on the Physics of Semiconductors, Moscow, 1968* (Nauka, Leningrad, 1968), Vol. 1, p. 312.
[47]C. R. Pidgeon, in *Handbook on Semiconductors,* edited by M. Balkanski (North-Holland, Amsterdam, 1980), Vol. 2, Chap. 5, pp. 223—328.
[48]L. I. Magarill and A. V. Chaplik, Pis'ma Zh. Eksp. Teor. Fiz. **40**, 301 (1984) [JETP Lett. **40**, 1089 (1985)].
[49]H. Heyszenau (unpublished).
[50]R. Lassnig and W. Zawadzki, Surf. Sci. **142**, 388 (1984).
[51]S. Das Sarma and B. A. Mason, Phys. Rev. B **31**, 5536 (1985).
[52]Staff of the Bateman Manuscript Project (A. Erdélyi, director), *Higher Transcendental Functions* (McGraw-Hill, New York, 1953), Vol. II, Chap. VIII, pp. 115—126.
[53]E. R. Smith, The American Mathematical Monthly **43**, 354 (1936).
[54]E. A. Kaner, N. M. Makarov, and I. M. Fuks, Zh. Eksp. Teor. Fiz. **55**, 931 (1968) [Sov. Phys.—JETP **28**, 483 (1969)].
[55]P. Dean, Proc. Cambridge Philos. Soc. **62**, 277 (1966).